

## COMMUNICATION

## Engineered Myosin VI Motors Reveal Minimal Structural Determinants of Directionality and Processivity

Jung-Chi Liao<sup>1,2</sup>, Mary Williard Elting<sup>2,3</sup>, Scott L. Delp<sup>1</sup>,  
James A. Spudich<sup>2</sup> and Zev Bryant<sup>1,2,4\*</sup>

<sup>1</sup>Department of Bioengineering,  
Stanford University, Stanford,  
CA 94305, USA

<sup>2</sup>Department of Biochemistry,  
Stanford University Medical  
Center, Stanford, CA 94305,  
USA

<sup>3</sup>Department of Applied Physics,  
Stanford University, Stanford,  
CA 94305, USA

<sup>4</sup>Department of Structural  
Biology, Stanford University  
Medical Center, Stanford,  
CA 94305, USA

Received 17 April 2009;  
received in revised form  
11 July 2009;  
accepted 16 July 2009

Edited by R. Craig

Myosins have diverse mechanical properties reflecting a range of cellular roles. A major challenge is to understand the structural basis for generating novel functions from a common motor core. Myosin VI (M6) is specialized for processive motion toward the (–) end of actin filaments. We have used engineered M6 motors to test and refine the “redirected power stroke” model for (–) end directionality and to explore poorly understood structural requirements for processive stepping. Guided by crystal structures and molecular modeling, we fused artificial lever arms to the catalytic head of M6 at several positions, retaining varying amounts of native structure. We found that an 18-residue  $\alpha$ -helical insert is sufficient to reverse the directionality of the motor, with no requirement for any calmodulin light chains. Further, we observed robust processive stepping of motors with artificial lever arms, demonstrating that processivity can arise without optimizing lever arm composition or mechanics.

© 2009 Published by Elsevier Ltd.

Members of the myosin superfamily have acquired specialized mechanical adaptations to perform cellular functions ranging from vesicle transport to muscle contraction. Myosin VI (M6) moves toward the (–) end of the actin filament, in the opposite direction from all other characterized myosins.<sup>1</sup> Additionally, unlike muscle myosin II, individual dimers of M6 can travel processively for many steps before detaching from the filament.<sup>2</sup> The determinants of M6 directionality and the

mechanism of M6 processivity have recently been the subjects of considerable scrutiny.<sup>3–10</sup>

Structural and functional studies have converged on a redirected power stroke model to explain directional reversal in M6. According to current formulations of the power stroke or swinging cross-bridge model of myosin force generation,<sup>11</sup> conformational changes at the nucleotide binding site are propagated through the catalytic head, driving a large rotation of the converter domain. This rotation is amplified by a rigid lever arm structure extending from the final helix of the converter. An X-ray crystal structure of the M6 post-stroke state showed that the lever arm emerges at an angle that differs from (+) end-directed myosins by  $\sim 120^\circ$  due to the presence of a unique insert in M6 following the converter (Fig. 1a).<sup>9</sup> Engineered motors truncated before the unique insert show (+) end-directed motion,<sup>3</sup> as do chimeric motors in which M6 is fused immediately after the converter to the lever

\*Corresponding author. E-mail address:  
[zevry@stanford.edu](mailto:zevry@stanford.edu).

Present address: J.-C. Liao, Department of Mechanical Engineering, Columbia University, New York, NY 10027, USA.

Abbreviations used: M6, myosin VI; MD, molecular dynamics.

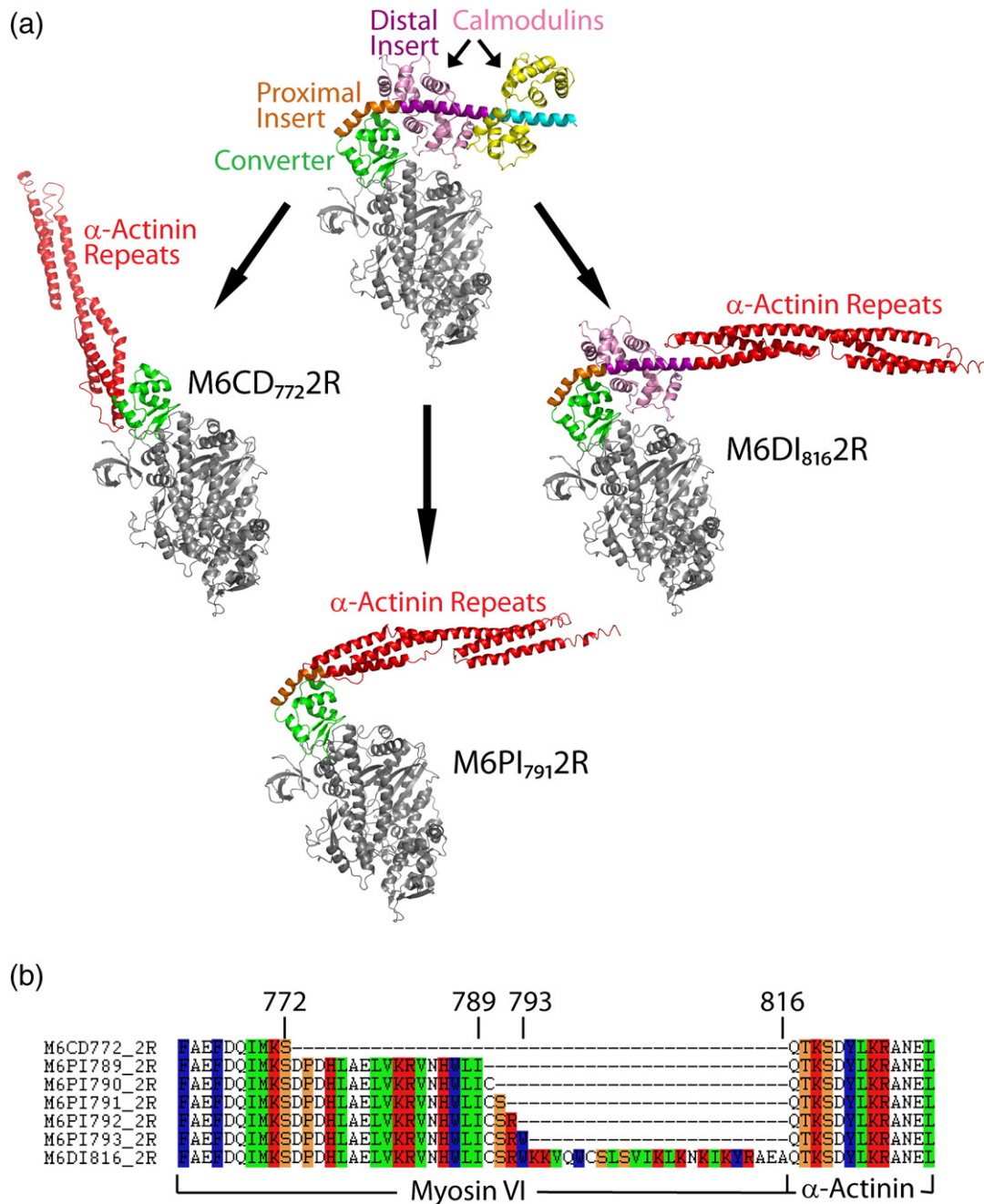


**Fig. 1.** Design of engineered M6 motors. (a) Post-stroke structure of M6 (top) and model structures of chimeric constructs with artificial lever arms derived from  $\alpha$ -actinin. In M6CD<sub>772</sub>R, spectrin repeats from  $\alpha$ -actinin are fused after the converter domain but prior to the unique insert; in M6PI<sub>791</sub>R, the  $\alpha$ -actinin repeats are fused immediately after the proximal part of the unique insert; in M6DI<sub>816</sub>R, the  $\alpha$ -actinin repeats are fused after the distal part of the insert. (b) Amino acid sequences of chimeric constructs at the site of fusion between myosin and  $\alpha$ -actinin.

77 arm from myosin V.<sup>5</sup> These studies demonstrate that  
 78 redirection of the lever arm mediated by the unique  
 79 insert is essential for (-) end directionality.

80 An examination of stroke sizes for a series of  
 81 truncated M6 constructs led to a model in which the  
 82 redirected lever arm rotates by  $\sim 180^\circ$  during the  
 83 power stroke.<sup>3</sup> This model was supported by a sub-  
 84 sequent crystal structure of the putative pre-stroke  
 85 state.<sup>10</sup> However, the pre-stroke crystal structure  
 86 was obtained using a fragment of M6 that lacks the  
 87 distal part of the unique insert and its associated

88 stabilizing light chain. The lever arm angle in this  
 89 structure could only be deduced by modeling the  
 90 missing distal insert. The functional relevance of the  
 91 crystallized conformation, which contains large and  
 92 surprising rearrangements of the converter domain,  
 93 must remain tentative in the absence of experiments  
 94 showing that the proximal part of the unique insert is  
 95 sufficient to correctly position a lever arm for (-)  
 96 end-directed motion.

97 Functional replacement of the myosin II lever arm  
 98 with rigid three-helix bundles derived from  $\alpha$ -actinin

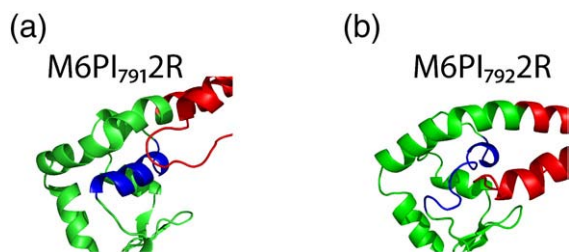


**Fig. 2.** MD simulations showing predicted differences in stability between alternative proximal insert fusion constructs that differ by one residue in the placement of the fusion point. (a) A snapshot from a simulation of M6PI<sub>791</sub>2R shows stable local structure in the converter domain. (b) A snapshot from a simulation of M6PI<sub>792</sub>2R shows a denatured  $\alpha$ -helix (blue) in the converter domain.

99 provided critical tests of the swinging cross-bridge  
100 model for myosin II.<sup>12,13</sup> Here, we have used an  
101 extension of this strategy to challenge and refine the  
102 redirected power stroke model for M6 directionality.  
103 We have characterized M6 constructs in which  $\alpha$ -  
104 actinin lever arms have been fused at several  
105 different locations following the converter domain.  
106 We include constructs in which the lever arm is fused  
107 immediately following the proximal part of the  
108 unique insert, probing whether this structure is  
109 sufficient for (-) end directionality.

110 Our strategy also provides a means to test models  
111 relating structure to processivity. Dimers of M6 have  
112 been shown to move processively with a hand-over-  
113 hand mechanism<sup>8,14</sup> thought to depend on coordina-  
114 tion mediated by strain in the lever arms.<sup>15</sup> By replac-  
115 ing lever arms with alternative structural elements,  
116 we can directly test the effects on processivity of  
117 varying geometric and mechanical parameters in the  
118 dimer.

119 We designed chimeric constructs in which an  
120 artificial lever arm<sup>12,16</sup> (two spectrin repeats from  
121 *Dictyostelium*  $\alpha$ -actinin, designated 2R) was fused to  
122 M6 at one of three locations (Fig. 1a and b): (1) after  
123 the converter domain but prior to the unique insert,  
124 M6CD<sub>772</sub>2R; (2) immediately after the proximal part  
125 of the unique insert, M6PI<sub>791</sub>2R; and (3) after the  
126 distal part of the insert, M6DI<sub>816</sub>2R. (Subscripts indi-  
127 cate the residue number of the last native M6 amino  
128 acid prior to the 2R junction.) M6CD<sub>772</sub>2R is pre-

dicted to have a lever arm orientation similar to  
129 myosin II. The longer constructs are predicted to  
130 yield lever arm orientations similar to native M6 but  
131 with differences in lever arm stability and mechanics  
132 due to the replacement of one or both native  
133 calmodulin-binding domains.  
134

135 Precise fusion points at the level of amino acid  
136 residues were chosen with the aid of molecular  
137 modeling. For the constructs fused after the prox-  
138 imal part of the unique insert, five possible adjacent  
139 fusion points were modeled. Models of M6PI<sub>789</sub>2R  
140 and M6PI<sub>793</sub>2R showed steric collisions between the  
141 converter and the artificial lever arm. Initial models  
142 of M6PI<sub>790</sub>2R, M6PI<sub>791</sub>2R, and M6PI<sub>792</sub>2R were free  
143 of structural collisions, but molecular dynamics  
144 (MD) simulations for the three models predicted  
145 differing stabilities of local structures (Fig. 2 and  
146 Supplemental Movies S1 and S2). M6PI<sub>790</sub>2R and  
147 M6PI<sub>791</sub>2R remained stable for 5 ns of MD simula-  
148 tion. In contrast, a key  $\alpha$ -helix in the converter  
149 domain of M6PI<sub>792</sub>2R became disordered during all-  
150 atom simulations. Thus, our models predicted that  
151 only two of these five fusions should retain func-  
152 tional lever arms: M6PI<sub>790</sub>2R and M6PI<sub>791</sub>2R.

153 A total of seven monomeric fusion constructs were  
154 expressed, purified, and assayed for motility, velo-  
155 city, and directionality using dual-labeled gliding  
156 filament assays. In addition, the dimeric artificial  
157 lever arm construct M6DI<sub>816</sub>2RGCN4 was generated  
158 by fusion of M6DI<sub>816</sub>2R to the medial tail region of  
159 M6 followed by the leucine zipper GCN4 in order to  
160 ensure dimerization. This construct was expressed  
161 and assayed for processivity using single fluoro-  
162 phore tracking.

163 *Constructs fused after the converter or after the unique*  
164 *insert are motile and have the expected directionalities.*  
165 M6CD<sub>772</sub>2R shows (+) end-directed motion in dual-  
166 labeled gliding filament assays (Fig. 3a and Table 1;  
167 Movie S3), consistent with its predicted structural  
168 similarity to myosin II. M6DI<sub>816</sub>2R retains the entire  
169 unique insert and has an extended lever arm and was  
170 thus predicted to show rapid (-) end-directed  
171 motion. Assays (Fig. 3b; Movie S4) show the  
172 expected movement at an average velocity of  
173 -110 nm/s (Table 1), compared with -45 nm/s for  
174 a construct truncated after the unique insert alone.<sup>3</sup>

175 *All-atom modeling correctly predicts functional fusion*  
176 *sites.* We tested all five constructs fused after the

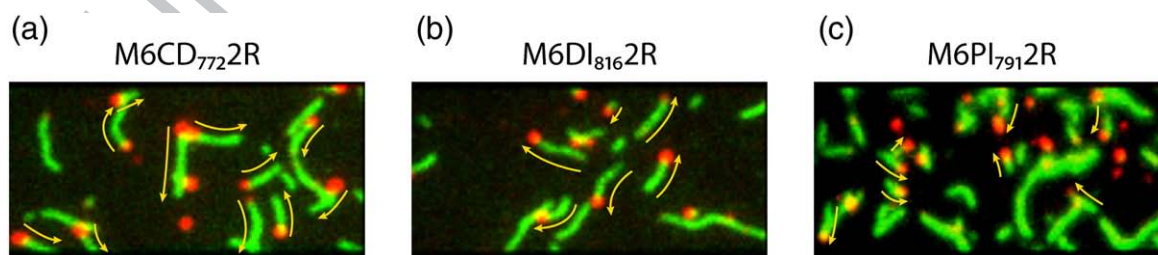


**Fig. 3.** Images from dual-labeled gliding filament assays showing the directionality of engineered constructs (see also Supplemental Movies S3–S7). Tetramethylrhodamine-phalloidin-labeled actin filaments are false-colored in green; Cy5-labeled (+) ends appear as red dots. The direction of gliding movement is indicated by yellow arrows. (a) M6CD<sub>772</sub>2R shows (+) end-directed movement, while (b) M6DI<sub>816</sub>2R and (c) M6PI<sub>791</sub>2R show (-) end-directed movement.



**Table 1.** Gliding filament results for engineered M6 motors

	M6CD <sub>772</sub> 2R	M6PI <sub>791</sub> 2R	M6DI <sub>816</sub> 2R
Directionality	(+) end (51/51 filaments)	(-) end (64/65 filaments)	(-) end (86/89 filaments)
Velocity	+40.64±1.92 nm/s ( <i>n</i> =44)	-29.03±1.39 nm/s ( <i>n</i> =32)	-110.66±4.42 nm/s ( <i>n</i> =51)

proximal part of the unique insert and observed only stationary actin filaments in assays of the three constructs (M6PI<sub>789</sub>2R, M6PI<sub>792</sub>2R, and M6PI<sub>793</sub>2R) showing steric clashes or helix instability in MD simulations (Movie S5). Both of the constructs that remained stable in MD simulations (M6PI<sub>790</sub>2R and M6PI<sub>791</sub>2R) were motile (Movies S6 and S7).

Constructs fused after the proximal part of the unique insert are (-) end directed, showing that the distal part of the insert is dispensable for directionality reversal. M6PI<sub>790</sub>2R and M6PI<sub>791</sub>2R show robust (-) end-directed motion in gliding filament assays (Fig. 3c and Table 1). These constructs move in the opposite direction from M6CD<sub>772</sub>2R due to the insertion of only 18–19 amino acids that form a proline kink and a short  $\alpha$ -helical section, without any stabilizing light chains.

Table 1 summarizes gliding filament results for monomeric engineered M6 motors. Directionalities agree with predictions and demonstrate that a short  $\alpha$ -helical insert is sufficient to reverse the directionality of the motor. In these assays, polarity-labeled

filaments occasionally become mislabeled, likely due to loss of the gelsolin cap on some Cy5-actin seeds.<sup>17</sup> This explains results with M6PI<sub>791</sub>2R and M6DI<sub>816</sub>2R, in which fewer than 100% of filaments were scored as (-) end directed. As expected, the highest gliding filament velocity is seen for M6DI<sub>816</sub>2R, which has the longest lever arm length (Fig. 1). M6CD<sub>772</sub>2R and M6PI<sub>791</sub>2R are expected to have relatively lower velocities due to shortened stroke sizes. Further reductions in velocity for the shortened constructs may occur due to increased actin attachment times, as seen previously for truncated M6 constructs lacking light-chain binding regions.<sup>3</sup>

Artificial lever arms can support processive movement. The dimeric construct M6DI<sub>816</sub>2RGCN4 was tested for processivity and compared to M6-GCN4 control (Fig. 4a and b). We used total internal reflection fluorescence imaging to track the movement of individual tetramethylrhodamine-labeled dimers on actin filaments (Movie S8). M6DI<sub>816</sub>2RGCN4 showed processive movement similar to control

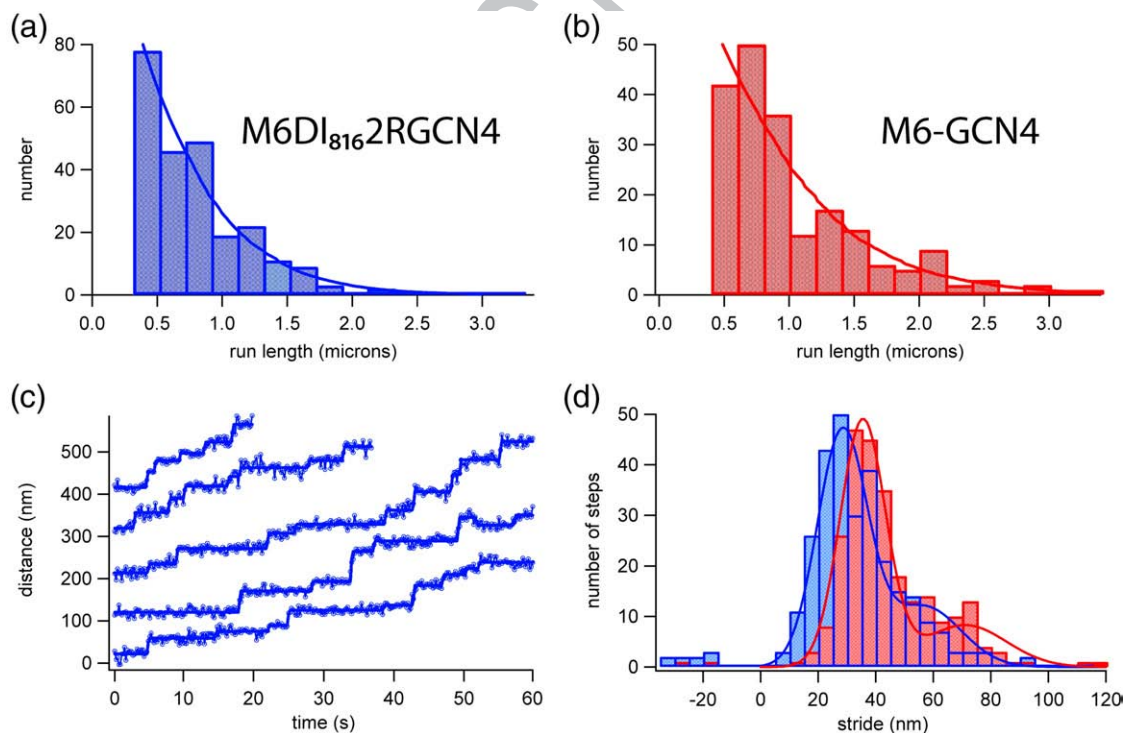


**Fig. 4.** Processive data from single-fluorophore tracking of tetramethylrhodamine-labeled dimeric constructs. (a and b) Histograms of processive run lengths for a dimeric M6 with artificial lever arms, M6DI<sub>816</sub>2RGCN4 (mean run length, 590±50 nm; *n*=243) and control M6-GCN4 (854±91 nm; *n*=199). (c) Sample stepping traces for M6DI<sub>816</sub>2RGCN4. Blue circles, data from fluorophore localization; solid blue lines, step-finding fits. (d) Stride histograms show that M6DI<sub>816</sub>2RGCN4 (blue) has a slightly shorter stride (28.4±0.5 nm) than M6-GCN4 (red) (35.5±0.5 nm).

221 dimeric M6-GCN4, with run lengths approximately  
222 70% as long as those of the control. Stepwise motion  
223 was detected during processive runs for both M6-  
224 GCN4 and M6DI<sub>816</sub>2RGCN4 (Fig. 4c), allowing us to  
225 measure the distribution of stride sizes (Fig. 4d). As  
226 expected from the extended lever arm design,  
227 M6DI<sub>816</sub>2RGCN4 stepped along the actin filament  
228 with long strides (28.4±0.5 nm). However, the peak  
229 stride size for M6DI<sub>816</sub>2RGCN4 was significantly  
230 smaller than that for control M6-GCN4 (35.5±0.5 nm),  
231 reflecting differences in lever arm geometry.

232 Directionality reversal in M6 was previously  
233 shown to depend on the presence of the 50-residue  
234 unique insert and its associated calmodulin light  
235 chain.<sup>3,5</sup> This light chain makes extensive contacts  
236 with the converter domain in the native M6 struc-  
237 ture, suggesting that it might play an important  
238 structural role in redirection of the lever arm.<sup>9</sup>  
239 However, we have shown here that the light chain  
240 and the distal part of the unique insert are dis-  
241 pensable for directionality reversal. Our results help  
242 validate the interpretation of a pre-stroke crystal  
243 structure for M6 in which the lever arm angle was  
244 assumed to be unperturbed by omission of the distal  
245 part of the unique insert and its associated light  
246 chain.<sup>10</sup> This provides additional support for a  
247 model in which the M6 lever arm is nearly per-  
248 pendicular to the actin filament and rotates close to  
249 180° during the power stroke.<sup>3,9,10,18</sup>

250 We have also shown that processive motion can be  
251 achieved in a dimeric myosin using artificial lever  
252 arms and without extensive optimization of lever  
253 arm geometry or mechanics. (Lack of geometric  
254 optimization in our constructs is underscored by the  
255 significantly shorter stride of the chimera, which  
256 fails to match the actin pseudo-repeat.) In most  
257 models of hand-over-hand motion, coordination of  
258 the two myosin heads is hypothesized to depend on  
259 internal strain generated when both heads are  
260 bound to the actin filament.<sup>15,19</sup> The mechanical  
261 properties of the lever arms might therefore be  
262 tuned for strain-mediated communication between  
263 the heads, and the lever arms might also be opti-  
264 mized for thermally sampling conformations during  
265 the binding site search that precedes front head  
266 reattachment. Computational models have led  
267 researchers to propose stringent mechanical require-  
268 ments for lever arms: Lan and Sun found that  
269 bending anisotropy was a key feature of computa-  
270 tional models for myosin V stepping.<sup>20</sup> Our findings  
271 imply that either coordination is robust to changes in  
272 lever arm composition or else coordination is  
273 relatively unimportant for processive motion. Indeed,  
274 as previously suggested,<sup>19</sup> dimers with indepen-  
275 dently cycling heads may theoretically be expected to  
276 show substantial processive motion, as long as the  
277 duty ratio of each monomer is high.

278 Finally, we note that while chimeric proteins can  
279 be powerful tools for structure/function studies,  
280 they must fold correctly in order to provide useful  
281 information. Here, we used all-atom molecular  
282 modeling to predict misfolding at junctions due to  
283 steric clashes or other unfavorable interactions. We

found that relatively simple atomistic computations  
helped discriminate between functional and non-  
functional chimeras. For chimeras involving exten-  
sive new domain interfaces, it may be necessary to  
apply sequence selection by structure-based protein  
design, as demonstrated earlier for a homing  
endonuclease.<sup>21</sup>

## Acknowledgements

We thank D. Parker, B. Spink, S. Sivaramakrishnan, S. Sutton, M. Footer, and H. Flyvbjerg for technical assistance and A. Dunn and R. Altman for helpful discussions. This work was supported by the National Institutes of Health (NIH) through the NIH Roadmap for Medical Research Grant U54 GM072970 (to J.-C.L., S.L.D., and J.A.S.). J.A.S. was supported by NIH Grant GM33289. Z.B. was supported by a Helen Hay Whitney Postdoctoral Fellowship and by NIH Grant DP2 OD004690. M.W.E. was supported by a National Science Foundation Graduate Research Fellowship.

## Supplementary Data

Supplementary data associated with this article can be found, in the online version, at [doi:10.1016/j.jmb.2009.07.046](https://doi.org/10.1016/j.jmb.2009.07.046)

## References

- Wells, A. L., Lin, A. W., Chen, L. Q., Safer, D., Cain, S. M., Hasson, T. *et al.* (1999). Myosin VI is an actin-based motor that moves backwards. *Nature*, **401**, 505–508.
- Rock, R. S., Rice, S. E., Wells, A. L., Purcell, T. J., Spudich, J. A. & Sweeney, H. L. (2001). Myosin VI is a processive motor with a large step size. *Proc. Natl Acad. Sci. USA*, **98**, 13655–13659.
- Bryant, Z., Altman, D. & Spudich, J. A. (2007). The power stroke of myosin VI and the basis of reverse directionality. *Proc. Natl Acad. Sci. USA*, **104**, 772–777.
- Iwaki, M., Tanaka, H., Iwane, A. H., Katayama, E., Ikebe, M. & Yanagida, T. (2006). Cargo-binding makes a wild-type single-headed myosin-VI move processively. *Biophys. J.* **90**, 3643–3652.
- Park, H., Li, A., Chen, L. Q., Houdusse, A., Selvin, P. R. & Sweeney, H. L. (2007). The unique insert at the end of the myosin VI motor is the sole determinant of directionality. *Proc. Natl Acad. Sci. USA*, **104**, 778–783.
- Park, H., Ramamurthy, B., Travaglia, M., Safer, D., Chen, L. Q., Franzini-Armstrong, C. *et al.* (2006). Full-length myosin VI dimerizes and moves processively along actin filaments upon monomer clustering. *Mol. Cell*, **21**, 331–336.
- Rock, R. S., Ramamurthy, B., Dunn, A. R., Beccafico, S., Rami, B. R., Morris, C. *et al.* (2005). A flexible domain is essential for the large step size and processivity of myosin VI. *Mol. Cell*, **17**, 603–609.
- Yildiz, A., Park, H., Safer, D., Yang, Z., Chen, L. Q., Selvin, P. R. & Sweeney, H. L. (2004). Myosin VI steps

- 339 via a hand-over-hand mechanism with its lever arm  
 340 undergoing fluctuations when attached to actin. *J. Biol.*  
 341 *Chem.* **279**, 37223–37226.
- 342 9. Menetrey, J., Bahloul, A., Wells, A. L., Yengo, C. M.,  
 343 Morris, C. A., Sweeney, H. L. & Houdusse, A. (2005).  
 344 The structure of the myosin VI motor reveals the  
 345 mechanism of directionality reversal. *Nature*, **435**,  
 346 779–785.
- 347 10. Menetrey, J., Llinas, P., Mukherjee, M., Sweeney, H. L.  
 348 & Houdusse, A. (2007). The structural basis for the  
 349 large powerstroke of myosin VI. *Cell*, **131**, 300–308.
- 350 11. Holmes, K. C., Schroder, R. R., Sweeney, H. L. &  
 351 Houdusse, A. (2004). The structure of the rigor  
 352 complex and its implications for the power stroke.  
 353 *Philos. Trans. R. Soc. London, Ser. B*, **359**, 1819–1828.
- 354 12. Anson, M., Geeves, M. A., Kurzawa, S. E. & Manstein,  
 355 D. J. (1996). Myosin motors with artificial lever arms.  
 356 *EMBO J.* **15**, 6069–6074.
- 357 13. Ruff, C., Furch, M., Brenner, B., Manstein, D. J. &  
 358 Meyhofer, E. (2001). Single-molecule tracking of  
 359 myosins with genetically engineered amplifier  
 360 domains. *Nat. Struct. Biol.* **8**, 226–229.
- 361 14. Okten, Z., Churchman, L. S., Rock, R. S. & Spudich,  
 362 J. A. (2004). Myosin VI walks hand-over-hand along  
 363 actin. *Nat. Struct. Mol. Biol.* **11**, 884–887.
- 364 15. Sweeney, H. L., Park, H., Zong, A. B., Yang, Z., Selvin,  
 365 P. R. & Rosenfeld, S. S. (2007). How myosin VI  
 366 coordinates its heads during processive movement.  
 367 *EMBO J.* **26**, 2682–2692.
- 368 16. Kliche, W., Fujita-Becker, S., Kollmar, M., Manstein,  
 369 D. J. & Kull, F. J. (2001). Structure of a genetically  
 370 engineered molecular motor. *EMBO J.* **20**, 40–46.
- 371 17. O'Connell, C. B. & Mooseker, M. S. (2003). Native  
 372 myosin-IXb is a plus-, not a minus-end-directed  
 373 motor. *Nat. Cell Biol.* **5**, 171–172.
- 374 18. Sun, Y., Schroeder, H. W., 3rd, Beausang, J. F.,  
 375 Homma, K., Ikebe, M. & Goldman, Y. E. (2007).  
 376 Myosin VI walks “wiggly” on actin with large and  
 377 variable tilting. *Mol. Cell*, **28**, 954–964.
- 378 19. Veigel, C., Wang, F., Bartoo, M. L., Sellers, J. R. &  
 379 Molloy, J. E. (2002). The gated gait of the processive  
 380 molecular motor, myosin V. *Nat. Cell Biol.* **4**, 59–65.
- 381 20. Lan, G. & Sun, S. X. (2006). Flexible light-chain  
 382 and helical structure of F-actin explain the move-  
 383 ment and step size of myosin-VI. *Biophys. J.* **91**,  
 384 4002–4013.
- 385 21. Chevalier, B. S., Kortemme, T., Chadsey, M. S., Baker,  
 386 D., Monnat, R. J. & Stoddard, B. L. (2002). Design,  
 387 activity, and structure of a highly specific artificial  
 388 endonuclease. *Mol. Cell*, **10**, 895–905.